HAL
open science

# Simultaneous two-channel MR imaging, single voxel spectroscopy and chemical shift imaging by reconfiguration of a 'standard' Biospec spectrometer

A.-L. Perrier, H. Ratiney, A. Rengle, D. Grenier, O. Beuf

## To cite this version:

A.-L. Perrier, H. Ratiney, A. Rengle, D. Grenier, O. Beuf. Simultaneous two-channel MR imaging, single voxel spectroscopy and chemical shift imaging by reconfiguration of a 'standard' Biospec spectrometer. Biomedical imaging and intervention journal, 2013, 9 (2), pp.e9. 10.2349/biij.9.2.e9 . hal-00847709

**HAL Id: hal-00847709**

**https://hal.science/hal-00847709v1**

Submitted on 19 Jun 2018

**HAL** is a multi-disciplinary open access archive for the deposit and dissemination of scientific research documents, whether they are published or not. The documents may come from teaching and research institutions in France or abroad, or from public or private research centers.

L'archive ouverte pluridisciplinaire **HAL**, est destinée au dépôt et à la diffusion de documents scientifiques de niveau recherche, publiés ou non, émanant des établissements d'enseignement et de recherche français ou étrangers, des laboratoires publics ou privés.

# Simultaneous two-channel MR imaging, single voxel spectroscopy and chemical shift imaging by reconfiguration of a ‘standard’ BioSpec® spectrometer

Perrier AL*, Ratiney H, Rengle A, Grenier D, Beuf O

*Université de Lyon, CREATIS; CNRS UMR 5220; Inserm U1044; INSA-Lyon; Université Lyon 1, Villeurbanne, France*

Received 11 July 2012; received in revised form 12 January 2013; accepted 23 January 2013

**ABSTRACT**

Simultaneous two-channel array proton imaging, single voxel PRESS and CSI acquisitions were demonstrated after reconfiguration and minimum hardware modification of a standard 4.7T BioSpec® spectrometer. Validation of the reconfiguration was assessed in phantoms and in a mouse brain. The modified configuration used the X-channel exhibiting similar SNR performances compared to the $^{1}$H-channel. The SNR gain for the two-channel array coil was up to 1.3 compared to the SNR obtained with a reference surface coil. Compared to regular two-element coil with quadrature combination, the SNR was improved with an additional gain of 1.3. These modifications could also be applied for any X-nucleus. © 2013 Biomedical Imaging and Intervention Journal. All rights reserved.

## INTRODUCTION

The advantages of phased-array coil imaging on clinical MR systems have gained relevance in many applications. In the small animal imaging field, the interest for this concept has grown. Array-coil imaging is an advanced method to enhance the signal-to-noise ratio (SNR) using superior sensitivity of several small coil elements compared to a larger single element covering the same field of view (FOV) [1, 2]. This is accomplished by using an array of smaller diameter coils with intrinsic superior sensitivity to improve SNR performance compared to conventional resonators [3]. The data from the array coils are acquired simultaneously and independently from each other and then combined into a single dataset. Spectroscopic and imaging data can both benefit from such coils [4]. In the case of two channels only, the main difference between array and quadrature detection is that the quadrature region is, in general, not identical to the region of optimal sensitivity of two single coils with the exception of a coil pair with a tilt angle of 90 degrees [5]. Another major advantage of phased-array coils is the possibility of using parallel imaging techniques, such as SENSE [6] and GRAPPA [7], to accelerate the encoding process for spatial localisation, which is highly beneficial for spectroscopic imaging [8, 9] and to bring additional flexibility in applications requiring higher temporal resolution. Additionally, the multiple array of receiver coils has demonstrated that there is interest in using it for multiple-animal MRI [10, 11]. Although phased-array technology is standard on clinical systems, high field experimental systems with multiple receiver channels capabilities only became available few years ago and this feature on such systems remains expensive.

In this work, a ‘standard’ 4.7 T Bruker BioSpec® Avance II spectrometer with two broadband chains, one

* Corresponding author. Address: CREATIS, Site UCB Lyon1-ESCPE, 3, rue Victor Grignard, 69616 Villeurbanne cedex, France. E-mail: perrier@creatis.insa-lyon.fr (Anne-Laure Perrier). The content of this manuscript was partly presented at the 17th Annual Meeting of ISMRM, Hawaï, 2009.

dedicated to proton ($^{1}H$) and one dedicated to X nuclei (with X = $^{31}P$, $^{23}NA$, $^{13}C$, ...) was modified to allow simultaneous two-channel $^{1}H$ acquisitions. These modifications were validated *in-vitro* in a phantom as well as *in-vivo* on mice brain for imaging, with single voxel spectroscopy and chemical shift imaging using a home-made two-channel phased array coil operating at 200.3 MHz.

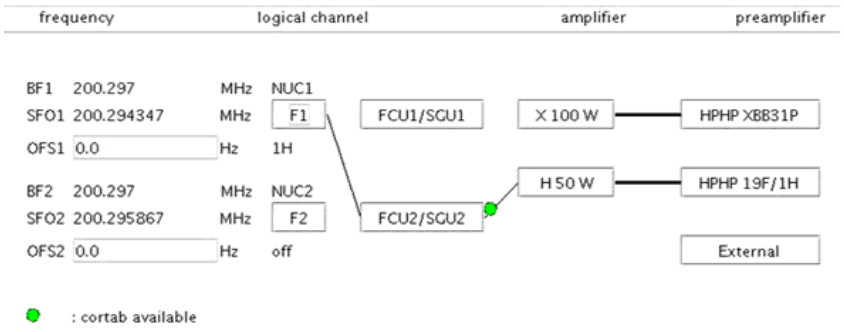


(a)

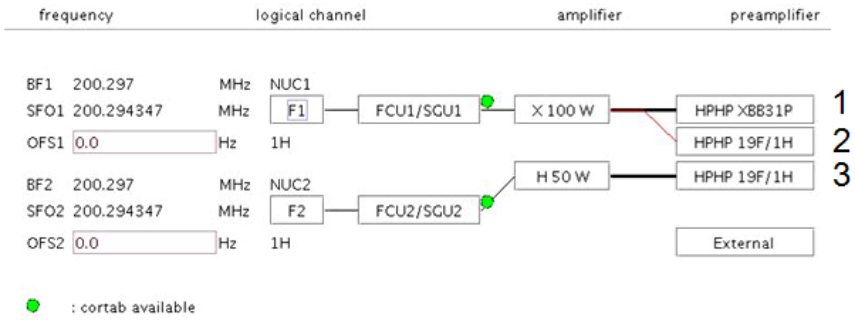


(b)

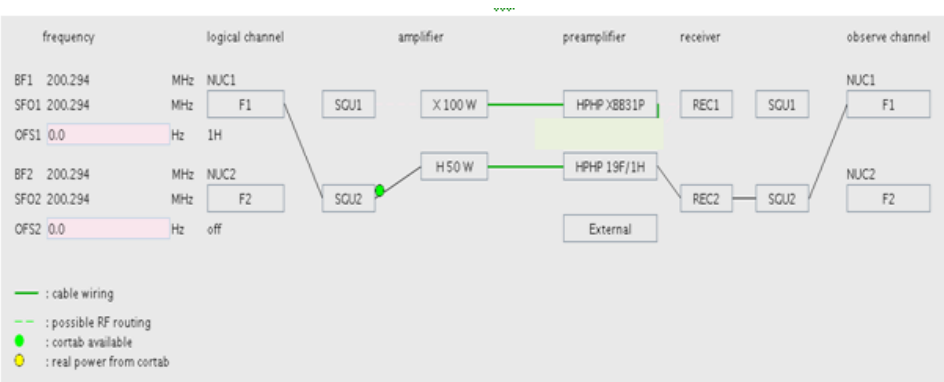


(c)

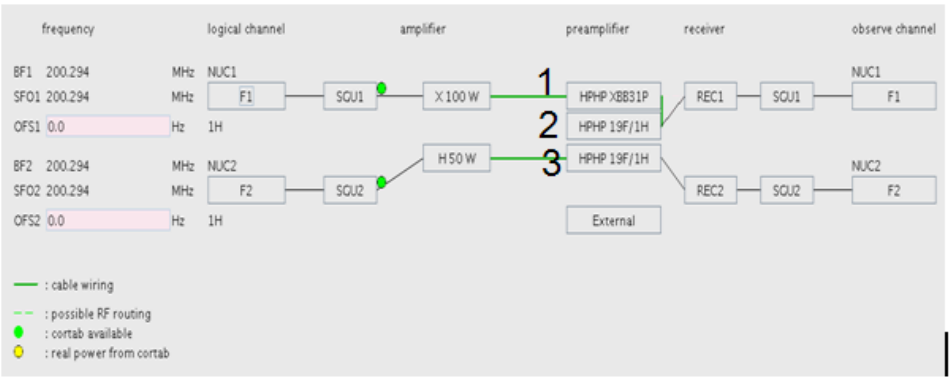


(d)

**Figure 1** The routing connection scheme displayed with PV4.0 (first raw) and PV5.0 (second raw) used for: the standard single channel proton acquisition (a, c); the simultaneous two-channel proton acquisition (b, d). In this latter configuration, a second preamplifier module was added to the standard BioSpec® spectrometer.

## MATERIALS AND METHODS

### *Spectrometer configuration*

The experiments were performed on a Bruker 4.7 T BioSpec® Avance II system (Bruker, Ettlingen, Germany) with a 270 mT/m maximum gradient amplitude available and a 100 mm clear bore diameter. A linear 72 mm inner diameter transmit birdcage coil (Rapid Biomedical, Würzburg, Germany) and a home-designed two-channel phased array receiver coil were used.

#### *Standard Spectrometer routing*

For a standard proton acquisition the routing defining the connections between the hardware parts involved in the acquisition pipeline is shown in Figure 1a. The RF transmit pulse is synthesised by the *Signal Generator Unit* (SGU2) and by the *Frequency Converter Unit* (FCU1) at the specified frequency. The synthesisers have to be assigned to logical channels F1 or F2. The RF pulse is then amplified by the dedicated proton amplifier (H50W) and sent to the transmit coil. The HPHP module consists mainly of a receiver low noise preamplifier optimised in a specific frequency range (19F/1H for example) with a *Transmit / Receive Switch* in *Single Coil Operation* mode. In *Cross Coil Operation* mode (case described here), the output of the transmit RF amplifier is directly connected to the volume transmit coil. In reception, the NMR signal picked up by the surface coils is transferred to REC/SGU2 units through the original 19F/1H preamplifier.

#### *Hardware Modifications*

In order to perform a simultaneous two-channel acquisition, the routing of the MRI spectrometer was modified according to Figure 1b and d. The excitation was performed using the X nucleus amplifier (though F1 logical channel) directly to the volume transmit coil. For reception, a second 19F/1H preamplifier module was added for the 2nd receiving channel (Figure 1b and d). The standard $^{1}$H-nucleus chain together with the X-nucleus chain, which was interconnected with this second proton preamplifier, were used. Hence, the two channels of the receiving coil were directly connected with the two 19F/1H preamplifier and signals were transferred to the REC/SGU 1 and 2 receivers.

#### *Software Modifications*

Using the Bruker Macro called “EditCoilConf” (in PV5.0 version only), a total of two coil configurations and two routings were defined to perform both wobble and two-channel acquisitions without having to declare a new study. The first configuration, used during the wobble procedure, is a linear volume coil connected with the preamplifier 3. This regular routing is mandatory to properly tune and match each coil element (Figure 1a and c). The second coil configuration is the two-channel surface coil mode achieved with one channel connected with “preamplifier 2 RF-in”, the other one connected with “preamplifier 3 RF-in” (Figure 1b and d).

The output of the X nucleus amplifier was linearised, for the proton frequency, by creating a correction table (cortab). This cortab file was used to correct the RF pulse power level non-linearity versus the pulse length. The methods including the pulse programmes were modified to activate the second receiver channel and handle the sum of squares reconstruction (for imaging only). Hence, for the MSME (i.e Multi Slice Multi Echo), FLASH (i.e Fast Low Agle SHot) and RARE (i.e Rapid Acquisition Relaxed Enhanced) imaging sequences and for spectroscopy the PRESS (i.e Point RESolved Spectroscopy) and CSI (i.e Chemical Shift Imaging) sequences were adapted for simultaneous two-channel acquisition. For each sequence (method), a pulse programme <sequence.2ch> was created starting from <sequence.4ch> files, provided by default to drive four receivers. Indeed, Bruker is able to provide an optional 4-receiver channel. In the <sequence.4ch> file, recp3 and recp4 code lines have to be put into comment. Hence, the pulse programme enables the second receiver: initialisation, start of acquisition, stop of acquisition and reset. The sequences were modified to use by default the new pulse programme associated to the new routing file. For imaging, the reconstruction part was also modified. The reconstruction was enabled in *User Mode*, to allow the sorting of data and reconstruction (each channel individually or sum of square of the two channels).

### *Two-channel coil interfacing*

The two-channel array coil was built on a Plexiglas™ cylinder with 21 mm outer diameter and 19 mm inner diameter. Each element consists of a rectangular single loop with $12 \times 16$ mm$^2$ internal and $15 \times 20$ mm$^2$ external dimensions (Figure 2a). One leg of this loop is common for the two elements. The decoupling of the two channels was achieved using a fixed decoupling capacitor on the common conductor of the two loops [12–14]. The value was experimentally adjusted to minimise the $|S_{12}|$ parameter between the two channels. The $|S_{12}|$ parameter is the transmission measure between the two channels representing coupling between the two loops. Both channels were tuned at 200.3 MHz corresponding to the proton’s resonance frequency at 4.7 T and matched to 50 Ω for this frequency using non-magnetic case A series 100 and 710 ATC capacitors (American Technical Ceramics, New York, USA). For fine-tuning and matching, variable capacitance diodes BB 149 (Philips Semiconductors, Eindhoven, Netherlands) driven with variable voltage were used. To decouple the array coil from the emitting coil, both coil channels have an active decoupling circuit with two parallel DH 80055 PIN diodes (Temex Ceramics, Pessac, France) (Figure 2a).

The fine-tuning/matching and actively decoupling circuit was designed to be interfaced and driven by the “Bruker Decoupling Box”. The Bruker Decoupling Box has two distinct parts, one committed to proton coils and the second to other X-nucleus coils. Each section

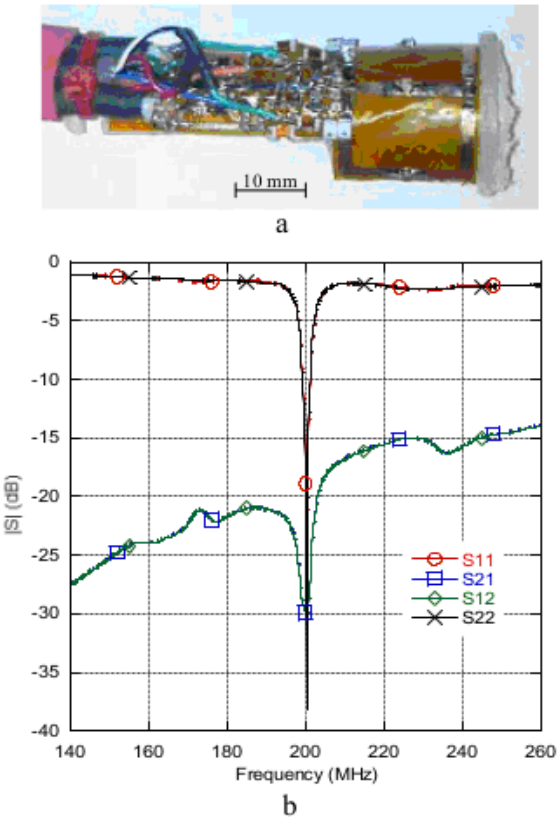


**Figure 2** Photograph of the two-channel phased-array coil used (a) and S-parameters measured with a cylindric fantomed loaded with 0.45% saline solution (b).

includes a decoupling signal for transmission coil and two set of adjustable voltage potentiometers to drive the variable capacitance for tuning and matching of proton and X-nucleus reception coils. The latter signals are delivered through a unique 14-pin connector. Then the first channel of our phased array coil was connected to pins used for the proton section ($1^{st}$ and $2^{nd}$ pins) and the second channel was connected to $8^{th}$ and $9^{th}$ pins usually used to other nucleus section. PIN diodes were biased using the $7^{th}$ pin, and the $6^{th}$ pin was grounded. Finally, the decoupling signal for the transmission coil was sourced from the twin connector from the X-nucleus section.

The home-designed phased-array coil was compared to a single channel 15 mm diameter multipurpose surface coil.

*MRI/MRS acquisitions*

Experimental tests were performed *in vitro*, firstly to characterise the designed array coil in terms of signal distribution and signal-to-noise ratio compared to the performances of a surface coil. Secondly, the two-channel acquisition which offers the ability of individually phasing the signals from each channel prior to their combination was compared to a pseudo quadrature acquisition. The quadrature condition was obtained by simply summing the output signals from the two coils assuming a constant 90-degree phase difference between them.

*In vitro*

The acquisitions were performed on two 18 mm inner diameter cylindrical phantoms containing a metabolite mixture (creatine (Cr), choline (Cho), γ-aminobutyric acid (GABA), glutamate (Glu), glutamine (Gln), N-acetylaspartate (NAA), taurine (Tau), lactate (Lac) and myo-inositol (Ins), pH = 7, 10 ml). For the first phantom used, the metabolite was at a concentration of 50 mM and dissolved in pure water. For the second phantom used for the chemical shift imaging acquisition, the metabolite was in agarose gel to reduce metabolite $T_1$ and at a concentration of 50mM, except for choline, which was at a concentration of 16 mM. The signal uniformity, the possible artifacts from electronic components, the efficiency of the decoupling methods and the SNR were then compared with a reference 15 mm diameter receive-only surface coil.

A $T_1$-weighted Spin-Echo (SE) sequence was used with the following parameters: FOV = 35 × 35 $mm^2$, 256 × 256 matrix size, 16 slices of 2 mm thickness, 50 kHz receiver bandwidth (rbw), TR/TE = 260/10.7 ms.

Localised spectroscopic acquisitions were performed using a short–echo time PRESS sequence ($T_R/T_E$ = 5000/20 ms; 4096 data-points; 4 kHz rbw; $T_{acq}$ = 21 min). The volume of interest (2.5 × 2 × 2 $mm^3$) was located as shown in Figure 3a. First- and second-order shim terms were adjusted using FASTMAP.

Chemical Shift Imaging acquisitions were performed using slice selective spin-echo sequence

(TR/TE = 2500/20 ms, 20 × 20 × 2 $mm^3$ FOV, 16 × 16 in-plane CSI matrix, 1024 data-points, bandwidth of 4 kHz, $T_{acq}$ = 21 min. with NEX = 2). Signal from the outer volume was suppressed by 6 blocks of saturation pulses interleaved in the water suppression pulses (VAPOR). To obtain estimates of coil sensitivities for the combination of the two-channel data, unsuppressed water spectra were acquired with the same acquisition parameters and NEX = 1 ($T_{acq}$ = 10 min).

*In vivo*

Ethical guidelines for experimental investigations with animals were followed, and the experimental protocol was approved by the Animal Ethics Committee of our institution. Prior to imaging, gaseous anesthesia was induced in an induction box with a mixed gas of air (30 % oxygen) at a concentration of 4 % isoflurane (Laboratoire Belamont, Boulogne Billancourt, France). The mouse was then placed in a supine position on a dedicated plastic bed and the anesthesia was maintained at 2 % isoflurane and administered at 0.4 $L.min^{-1}$ via a face cone mask. A respiratory sensor was placed on the animal's abdomen to monitor the respiration rate. Post-scanning, mice were kept under a heating light until complete recovery.

The home-designed phased-array coil and the 15 mm surface coil were placed on top of the skull. An axial $T_2$-weighted fat-suppressed (FS) RARE sequence was used with the following parameters: $T_R/T_E$ = 3500/70 ms; RARE factor = 8; 25 × 25 $mm^2$ FOV; 256 x 192 matrix; 17 slices; 1 mm slice thickness; 14 kHz rbw; $T_{acq}$ = 2 min 48 s.

Single voxel short–echo time PRESS sequence was performed using the same parameters used for *in vitro* experiments. The 2.5 × 2 × 2 $mm^3$ volume of interest was centred in the right hippocampus.

For chemical shifting imaging, the following parameters were used: $T_R/T_E$ = 1200/50 ms; 28 × 28 × 2 $mm^3$ FOV; 15 × 15 in-plane CSI matrix; 1024 data-points; 4 kHz rbw; $T_{acq}$ = 45 min. Signal from the outer volume was suppressed by many blocks of saturation pulses interleaved in the water suppression pulses (VAPOR). The positioning of the spatial saturation bands is an important issue to avoid fat contamination. First- and second-order shim terms were adjusted using FASTMAP. As for *in vitro* data acquisition, unsuppressed water spectra were acquired for coil sensitivity estimations with the same acquisition parameters and NEX = 1 ($T_{acq}$ =4 min 30 s);

*Processing and data analysis*

For imaging, the SNR (mean ± standard deviation) was calculated on the Region of Interest (ROI), defined *in vitro* as an equivalent area corresponding to the surface and the location of the mouse brain (Figure 3b). *In vivo*, the SNR was effectively measured in the mouse brain for a unique axial central slice located in the middle of the coil.

For both *in vivo* and *in vitro* NMR spectroscopy data from the two channels were combined using Matlab 7.4 (Mathworks Inc, Natick, MA, USA) in the time domain using linear combination of the complex signals weighted by sum of squares of coil intensity. Prior to the combination, the signals from the two channels were zero-order phase corrected. For each coil, the coil intensity weighting factor was obtained from the mean value of the first four absolute time-domain data points of the corresponding unsuppressed-water signal.

The SNR was calculated in the time domain as ratio of the estimated metabolite amplitude relative to the time-domain noise standard deviation (computed from the tail of the signal, i.e. when the signal is totally damped, typically here in the 10% last points). Note that the time domain metabolite amplitude, is, for a phased signal, the first point value of the metabolite signal, which corresponds, for singlet, to the metabolite peak area. The SNR was measured and reported for the main resonating singlets of total Cho ($N(CH_3)_3$, 3.2 ppm), total

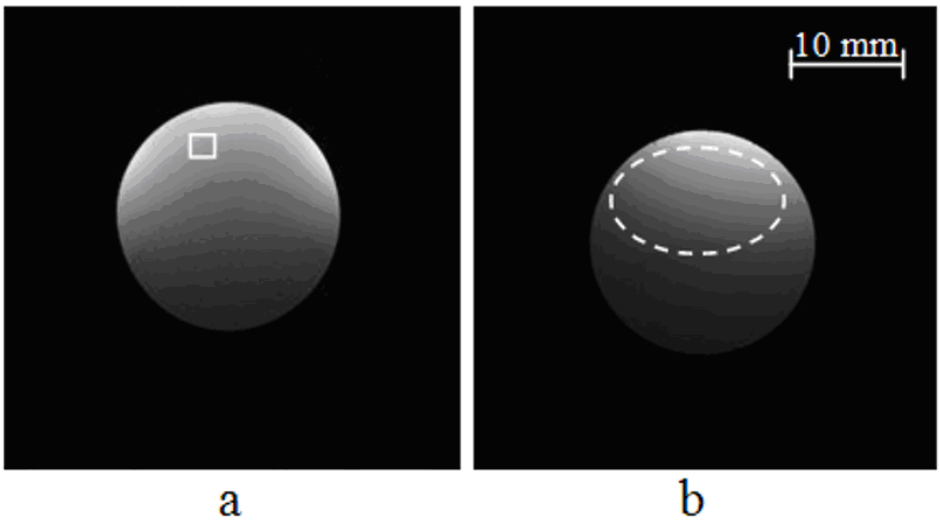


**Figure 3** Axial MR images obtained on a uniform cylindrical phantom containing the eleven metabolite solution with: (a) the two-channel phased-array coil and (b) the 15 mm surface coil. The location of the PRESS volume is shown in (a). The ROI used for SNR comparisons based on images is shown in (b).

Cr ($CH_3$, 3.03 ppm) and NAA ($CH_3$, 2.01 ppm), for which the signal intensity measurement is straightforward.

## RESULTS

The measured quality factor of the unloaded coil was 133 for every single channel. For a loaded coil, with a 17.5 mm diameter cylindrical phantom filled with 0.45 % NaCl solution, the quality factor decreased up to 127. The decoupling capacitor mounted on the circuit was about 56 pF. The isolation (decoupling) between the two channels measured with the $S_{12}$ parameter was -29 dB (Figure 2b).

### *In vitro*

No visible susceptibility artifacts from the components were depicted on images obtained with the uniform cylindrical phantom (Figure 3). The SNR gain for the two-channel array coil was up to 1.3 compared to the SNR obtained with the 15 mm diameter surface coil. Independently of the coil element connected, SNR measured on the X-channel was 5 to 10% higher compared to the $^1$H-channel.

For the PRESS acquisition, the SNR measured for three metabolites of interest, after combination of the two-channel, were 317, 111 and 113 compared to the surface coil with 192, 69 and 66 for Cho, Cr and NAA respectively. The average gain calculated on these three metabolites was 1.66 ± 0.05. Magnetic field homogeneities measured with both coils were comparable with a full width half maximum (FWHM) of 3.2 Hz (ranging from 2 to 5 Hz), indicating that the home-designed coil does not affect the line shape and line width.

For the CSI data, the SNR maps for the combination with complex weighting coefficients and for the pseudo quadrature combination are shown in Figure 4a and 4b respectively. A better signal intensity uniformity is obtained for the former case. Figure 4c depicts the map of the phase difference between the two channels, demonstrating that a 90-degree fixed difference assumption used in the pseudo-quadrature combination does not always hold. A voxel has been chosen in a region where the phase difference between the two channels is greater than 90 degrees (see the highlighted voxel in Figure 4d). The corresponding water spectra and water-suppressed spectra, which are individually phased, prior to the combination, for channel 1 and channel 2, and phased with the quadrature condition for the channel 2 are shown in Figure 4e and 4f. This illustrates the signal loss due to improper quadrature conditions. The comparison of the SNR maps showed that the SNR increased by a factor 1.2 ± 0.1 in average for the three quantified resonating singlets when combining the channels on a voxel per voxel relative phase correction base compared to the quadrature combination.

### *In vivo*

The mean SNR measured on $T_2$-weighted images in the mouse brain was 32.1 ± 4.0 for combined channels (27.3 ± 3.1 and 25.8 ± 3.2 for the first and second elements respectively). This represents about 25% SNR improvement compared to our 15 mm reference surface coil. Magnetic field homogeneities derived from PRESS spectra were comparable with usual experimental conditions with a full width half maximum (FWHM) of the NAA singlet of 13 Hz (ranging 12 to 15 Hz). The resonances of NAA, Cr, Cho, Glx were well detected (Figure 5). The CSI spectra are shown in Figure 5.

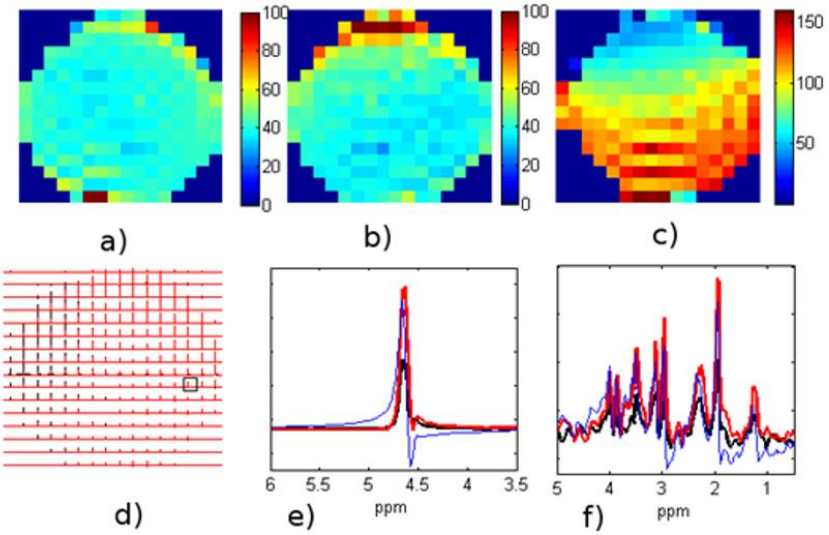


**Figure 4** Maps and spectra from an axial 16 × 6 proton MRSI acquisition obtained with a two coil array on a solution containing nine metabolites. SNR maps of the water peak obtained with (a) combination of the two channels (with complex weighting factors); (b) the pseudo quadrature combination. Notice the improved signal intensity uniformity in the first case; (c) Map in degree of the phase difference between the two channels; (d) the corresponding grid of spectra of channel 1 (black) and channel 2 (in red); (e,f) real part of the spectra from the voxel highlighted in (d) where the phase difference between the two channels is 128 degrees for the water peak and the water suppressed spectrum (in black the phased spectrum form the channel 1, in red the phased spectrum from the channel 2, in blue the spectrum from channel 2 phased in quadrature compared to channel 1).

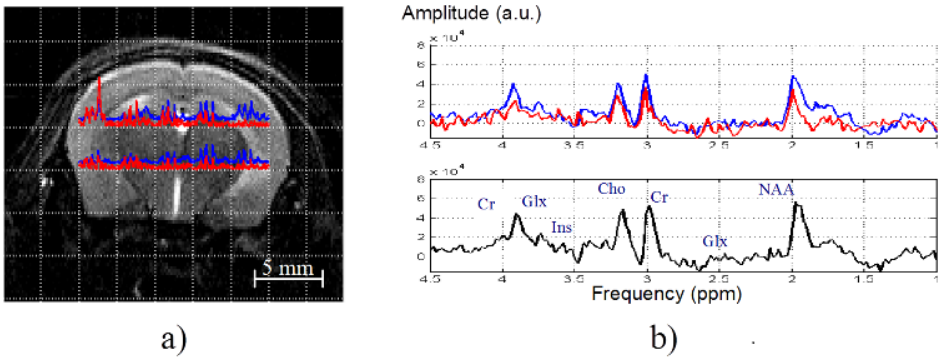


**Figure 5** The CSI spectra shown on a zoomed image of the mouse brain (a). For a voxel, the spectra are shown before (top) and after (bottom) the combination of the two channels (b). The resonances of NAA, Cr, Cho, Glx are well resolved. At TE=50ms, the contamination of the spectra by the macromolecules is reduced.

At $T_E = 40$ ms, the contamination of the spectra by the macromolecules is reduced. Both channels are equivalents with a mean SNR of 3.1 for NAA, or 2.9 for Cr for each channel and with a combined value of 3.7 for NAA or 3.5 for Cr. The combination of the channels, taking into account the individual phase for each voxel, results in higher metabolite SNR than the one derived from a quadrature combination. The gain is estimated by an averaged factor of $1.3 \pm 0.3$ computed over the 10 voxels of interest, highlighted in Figure 5.

## CONCLUSION

Simultaneous two-channel acquisition for imaging and spectroscopy, including CSI, was demonstrated after reconfiguration of a standard 4.7T BioSpec® spectrometer. The modifications were easy to implement. Only a second broadband RF transmit amplifier in the proton range is mandatory. The receiver chain also requires a second proton preamplifier. This preamplifier is optional with on board preamplifiers used for decoupling of coil elements by transforming into the NMR coil of the high input impedance of the preamplifier. Because the MR system is provided with sequences (methods) compatible with an optional 4-channel acquisition, sequence adaptation for two-channels is straightforward. In some cases, the modifications consisted of commenting on unused channels ($3^{rd}$ and $4^{th}$).

The modifications realised for proton multiple channel acquisitions could also be applied for any X-nucleus. The only limitations for acquiring other nucleus are hardware-related (dedicated coils and in case of phased array coils without on board preamplifiers, a HPHP module with preamplifier for the considered nucleus frequency).

Compared to quadrature detection coils, two-channel phased array coils offer first to phase signals from the two-channel independently, which is very beneficial from a SNR point of view as the phase difference is not 90 degrees over all the region of interest. It also offers the ability to use parallel acquisition techniques. Further steps will be to implement parallel acquisition techniques and to demonstrate the interest for small animal $^{1}$H imaging as well as for other nuclei such as $^{3}$He hyperpolarised gas imaging or DNP $^{13}$C. Another further step will be to implement parallel acquisition techniques together with k-space weighted CSI spin-echo sequence in order to improve SNR for a given scan time.

## ACKNOWLEDGEMENTS

We thank Dr Didier Wecker from Bruker Biospin for his support on routing and method modifications. This work was performed within the framework of the LABEX PRIMES (ANR-11-LABX-0063) of Université de Lyon, within the program “Investissements d'Avenir” (ANR-11-IDEX-0007) operated by the French National Research Agency (ANR).

## REFERENCES

1. Roemer PB, Edelstein WA, Hayes CE, Souza SP and Mueller OM. The NMR phased array. Magn Reson Med 1990; 16(2): 192–225.
2. Gareis D, Wichmann T, Lanz T, Melkus G, Horn M and Jakob PM. Mouse MRI using phased-array coils. NMR Biomed 2007; 20(3): 326–334.
3. Hoult DI and Richards RE. The signal-to-noise ratio of the nuclear magnetic resonance experiment. J Magn Reson 1976; 24(1): 71–85.
4. Wright SM and Wald LL. Theory and application of array coils in MR spectroscopy. NMR Biomed 1997; 10(8): 394–410.
5. Haase A, Odoj F, Von Kienlin M, Warnking J, Fidler F, Weisser A, Nittka M, Rommel E, Lanz T, Kalusche B and Griswold M. NMR probeheads for in vivo applications. Concepts Magn Reson 2000; 12(6): 361–388.
6. Pruessmann KP, Weiger M, Scheidegger MB and Boesiger P. SENSE: sensitivity encoding for fast MRI. Magn Reson Med 1999; 42(5): 952–962.
7. Griswold MA, Jakob PM, Heidemann RM, Nittka M, Jellus V, Wang J, Kiefer B and Haase A. Generalized autocalibrating partially parallel acquisitions (GRAPPA). Magn Reson Med 2002; 47(6): 1202–1210.
8. Lin FH, Tsai SY, Otazo R, Caprihan A, Wald LL, Belliveau JW and Posse S. Sensitivity-encoded (SENSE) proton echo-planar spectroscopic imaging (PEPSI) in the human brain. Magn Reson Med 2007; 57(2): 249–257.
9. Tsai SY, Otazo R, Posse S, Lin YR, Chung HW, Wald LL, Wiggins GC and Lin FH. Accelerated proton echo planar spectroscopic imaging (PEPSI) using GRAPPA with a 32-channel phased-array coil. Magn Reson Med 2008; 59(5): 989–998.
10. Ramirez MS, Esparza-Coss E and Bankson JA. Multiple-mouse MRI with multiple arrays of receive coils. Magn Reson Med 2010; 63(3): 803–810.
11. Beuf O, Jaillon F and Saint-Jalmes H. Small-animal MRI: signal-to-noise ratio comparison at 7 and 1.5 T with multiple-animal acquisition strategies. Magma 2006; 19(4): 202–208.
12. Rengle A, Armenean M, Bolbos R, Goebel JC, Pinzano-Watrin A,

Saint-Jalmes H, Gillet P and Beuf O. A dedicated two-channel phased-array receiver coil for high-resolution MRI of the rat knee cartilage at 7 T. IEEE Trans Biomed Eng 2009; 56(12): 2891–2897.
13. Zhang X and Webb A. Design of a capacitively decoupled transmit/receive NMR phased array for high field microscopy at 14.1 T. J Magn Reson 2004; 170(1): 149–155.
14. Perrier A, Grenier D, Pouzin A, Esclassan F, Ravel N, Litaudon P and Beuf O. Design of a two-channel NMR coil using an impedance transformation approach. Sensors Journal, IEEE 2012; 12(6): 1801–1808.